Proceedings of Global Power and Propulsion Society
ISSN-Nr: 2504-4400
GPPS Hong Kong 2023
October 17-19, 2023
www.gpps.global

GPPS-TC-2023-0056

Axial Compressor as eBooster for charging an Ultra-Lean-Burn Hydrogen Combustion Engine

Yannik Schulz
Leibniz Universität Hannover
y.schulz@tfd.uni-hannover.de
Hanover, Germany

Lukas Sagan
Technische Universität Braunschweig
l.sagan@tu-braunschweig.de
Brunswick, Germany

Joerg R. Seume
Leibniz Unviersität Hannover
seume@tfd.uni-hannover.de
Hanover, Germany

Peter Eilts
Technische Universität Braunschweig
p.eilts@tu-braunschweig.de
Brunswick, Germany

ABSTRACT

Hydrogen as a fuel in spark-ignition combustion engines provides an opportunity for using an ultra-lean-burn combustion strategy. This combustion concept has the advantage of ensuring a high thermal efficiency as well as ultra-low NOx emissions at the same time. This makes it an interesting concept, especially in the field of commercial vehicles. Providing these high pressure ratios while guaranteeing an acceptable boost pressure is challenging for charging systems. In order to face these requirements, an axial compressor eBooster stage is developed. The eBooster concept extends the operating range of a single-stage turbocharger. Otherwise, a complex and cost intensive two-stage configuration would be needed. The compressor is designed to operate for mass flow rates of 0.4 to 0.8 kg/s and total pressure ratios of up to 1.72. When operating the eBooster stage, the centrifugal compressor performance map is shifted towards higher mass flow rates by means of pre-compression. The compressor developed shows a peak isentropic efficiency of 82.8 % with high efficiencies (>78 %) for the whole operating range.

INTRODUCTION

With the Paris Climate Agreement, 196 signatory countries committed to limiting the global average temperature increase to 2 °C above pre-industrial level and to pursue measures to keep it below 1.5°C (Agreement (2015)). Therefore the EU adopted the goal of climate neutrality by 2050, which also implies climate neutral transportation. Currently the transportation sector makes up for about one quarter of greenhouse gas emissions in the EU that are energy-related (Plötz et al. (2021)). To cut these emissions down, alternative power-train systems are needed. As recently published studies have shown (Oung et al. (2022), Rezaei et al. (2021)) ultra-lean burn hydrogen combustion is a promising measure to achieve carbon neutrality, especially for heavy duty applications. By diluting the air-fuel mixture, the combustion temperature decreases, which finally results in a higher indicated engine efficiency. Also, the NO_X emissions can theoretically be reduced below detection limit because the formation of NO_X is strongly temperature dependent.

On the other hand, air dilution sets high requirements for a charging system. To achieve the same engine operating point at a higher relative air-to-fuel ratio λ, higher boost pressures are needed, while the exhaust provides lower available enthalpy. Additionally, the increased required engine air mass results in a large mass flow range that has to be covered by the used charging system. A single compressor does not seem to be sufficient for the boost pressure demand while maintaining high efficiency over the whole operating map. So far, a two stage charging system with variable turbine geometry is mandatory (Onorati et al. (2022)). However, this has several disadvantages - namely higher cost, increased installation space, more weight and higher control effort (Lee et al. (2008)).

The objective of this paper therefore is to develop a boosting system for ultra-lean-burn operation (λ=3.1) in a heavy duty hydrogen direct injection spark ignition engine over the whole operating range. This results in NO_X emissions below the optional standards of the California Air Resources Board (CARB) of 0.027$\frac{g}{kWh}$ (California Air Resources Board (2013)) without the use of exhaust gas after-treatment. Minimizing the costs and also time to market, a system design utilizing a commercially available turbocharger and an electrified axial compressor booster stage is chosen. The development procedure of the axial compressor will be presented in the present paper.

This work is licensed under **Attribution 4.0 International (CC BY 4.0)**
See: https://creativecommons.org/licenses/by/4.0/legalcode

METHODOLOGY

In order to determine the boundary conditions of the charging system and to derive a suitable compressor design, the following methodology is applied. First, a 0/1D engine model is set up to calculate the requirements for the charging system. After selecting a compressor system's layout and a design point, the 1D and 3D design is performed. Finally, the compressor performance map is calculated using computational fluid dynamics simulations (CFD).

1D ENGINE MODELING

A powerful tool to investigate the behaviour of an combustion engine within an early development stage is a 0/1D engine model. Within this paper, the simulation environment GT-Power (V2022, Build 1) is used. The engine model selected represents a generically (geometries based on similar sized diesel engine) derived inline six-cylinder H_2 engine within the 12l-class. This range of displacement is commonly used in commercial vehicle applications. Further the engine model is spark ignited (SI) and features direct injection (DI). Table 1 summarizes the relevant technical specifications of the engine.

Table 1 Technical specifications of the engine simulation model

Parameter	Unit	Value
Number of cylinder	-	Inline 6
Displacement	cm^3	12,149
Bore	mm	125
Stroke	mm	165
Compression ratio	-	11.5 : 1
Fuel	-	H_2 (gas)
Injection type	-	Direct injection

The H_2 combustion is modeled using the predictive SI-Turb combustion model in combination with the laminar flame speed model provided within the simulation environment. Calibration of the SI-Turb model is performed based on single-cylinder measurement data. The validated combustion model in then transferred into a generic full engine model. Further information about the development process of the combustion model used can be found in Rezaei et al. (2021) and Rieß et al. (2021).

In order to calculate boundary conditions for a charging system of a H_2 engine, some assumptions have to be made. In this case, the simple turbocharger model provided by GT-Suite is utilized. The simple TC model consists of the simple turbine and simple compressor object that may to be implemented instead of TC performance maps, when these are not derived yet. The simple turbine is characterized by an effective turbine diameter and an efficiency value. Here, this turbine efficiency is implicitly already accounting for effects of friction and heat transfer losses. Applying the two attributes, the software uses an orifice model to compute the turbine output power. The power is subsequently transferred to the simple compressor object, which is also characterized by a set efficiency value. Further details about the modeling theory of these objects can be found in Gamma Technologies GmbH (2022) and Heywood (2018).

Within this investigation the efficiency of the simple TC is set to a constant value of 64 %, applying efficiencies for the compressor and the turbine of 80 % each. These efficiencies represent realistic values for state of the art TC components within their region of maximum efficiency. Surely, the constant efficiency within the entire operating range of the components is not completely realistic. Nevertheless, it is a fair assumption to derive the preliminary boundary conditions for the charging system. Further, the simple turbine model is setup using a continuously variable turbine cross section, where the simple turbine diameter is controlled to meet the required engine load per engine operating point. The fuel injection is controlling the relative air-fuel ratio. Figure 1 summarises schematically the setup of the full engine model with its main components.

Further important assumptions for the design of the charging system are the engine operating points that have to be covered. Here, the engine map is chosen by a commercially available gas engine within similar displacement class (Fiat Powertrain (2013)). Based on the goal of achieving the NO_X emission limit set by the CARB regulation, a relative air/fuel ratio of 3.1 is chosen within the entire engine map. This value is found in preliminary simulations using the combustion model described. The resulting simulation matrix is illustrated in figure 2.

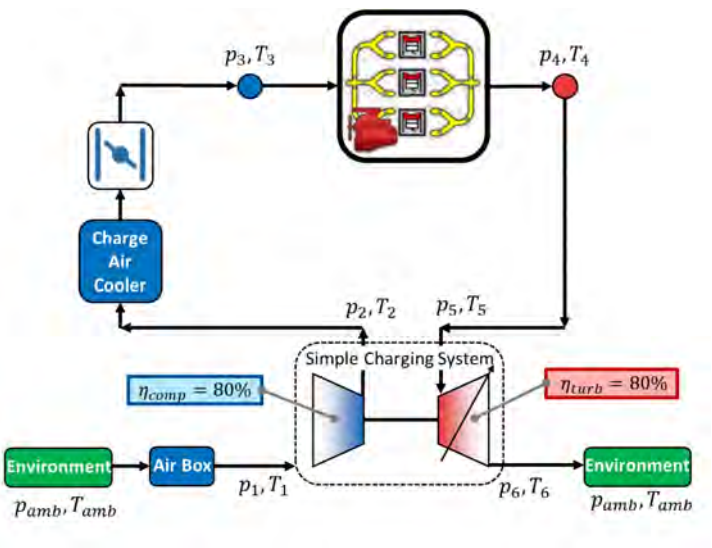

Figure 1 Schematic engine simulation model

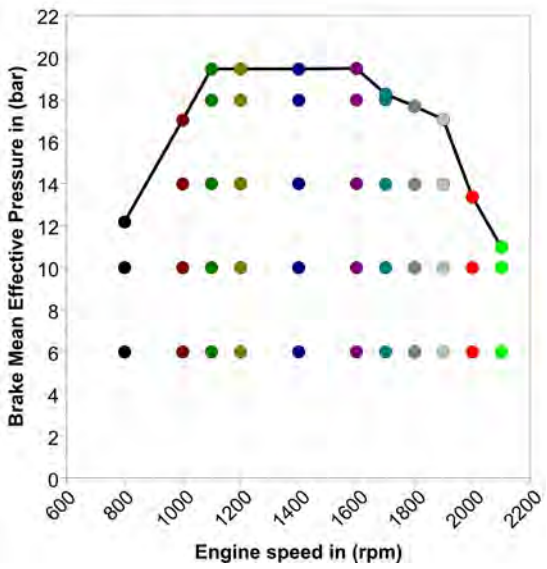

Figure 2 Engine simulation matrix ($\lambda = 3.1$)

Figure 3 illustrates the compressor requirements for the calculation using the simple turbocharger configuration with a constant TC efficiency of 64 % and a λ of 3.1. These show a high pressure ratio demand in combination with high mass flow rates and the surge limit sets high requirements for the compressor design. A single compressor does not seem to be sufficient for these requirements while maintaining high efficiency over the whole map.

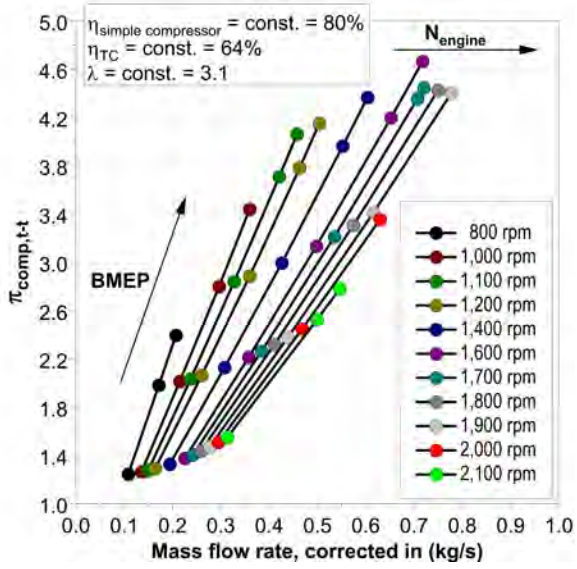

Figure 3 Requirements for the compressor derived from single-stage simple TC model (λ=3.1)

In order to overcome this challenging boost pressure demand, the boosting system layout as shown in figure 4 is chosen. It combines a traditional turbocharger with an electrically driven axial compressor placed upstream and which is not mechanically coupled. The electric energy to drive the electric motor (EM) is supposed to be supplied by the engine via the alternator.

The radial compressor is supposed to cover a significant amount of engine operating points in single stage operation, especially in the area of low end torque. The axial compressor is meant to be operated for points of higher load. This pre-compression provides two advantages: it reduces the corrected mass flow rate

$$\dot{m}_{cor} = \dot{m} \cdot \frac{p_{ref}}{p_{1,t}} \cdot \sqrt{\frac{T_{1,t}}{T_{ref}}} \tag{1}$$

which shifts the performance map of the centrifugal compressor towards higher mass flow rates and reduces the pressure ratio that the centrifugal compressor needs to deliver, shifting the operating point towards higher efficiencies. The use of

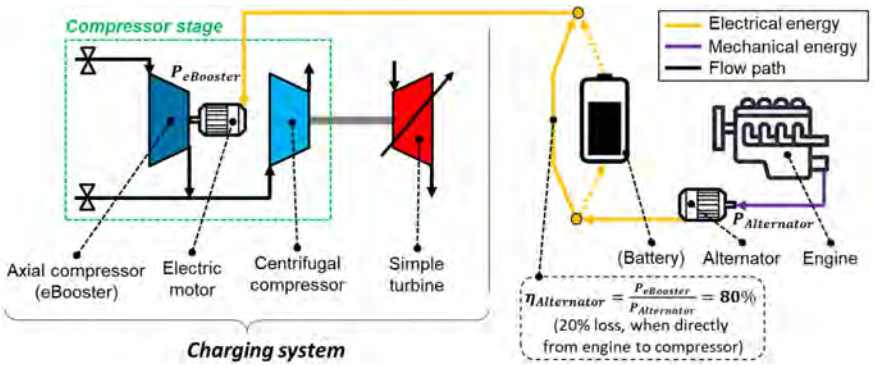

Figure 4 Boosting system concept.

an axial compressor therefore allows to reduce the size of the centrifugal compressor, reducing moment of inertia and improving transient response.

Next, the single stage system featuring simple compressor and simple turbine is replaced to derive requirements for the axial booster. Therefore, a suitable commercially available state-of-the-art centrifugal compressor (BorgWarner S300SX-E 83S74) is chosen. The compressor shows a peak efficiency of 78 %. This centrifugal compressor is supplemented by a simple compressor that is placed upstream of the radial compressor (fig. 4). The simple compressor representing the axial booster is modeled with a constant efficiency of 87 %, based on preliminary 1D throughflow simulation studies. The input power of the axial compressor is limited to 35 kW because it needs to be provided by an alternator which is driven by the engine. The alternator system is assumed to convert rotatory energy from the crankshaft to electric energy at $\eta_{Alternator}$=80 %. Hence, an increase in electrical power for the booster ultimately leads to an increasing parasitic loss and finally to an even greater required boost pressure demand. This effect is rooted in an increasing power demand at the turbine of the conventional TC, which leads to higher exhaust back pressure and ultimately to higher pumping losses of the engine. In order to find a trade-off between input power of the booster and achievable operating points of the engine, several axial compressor operating strategies are simulated with the simple axial booster (fig. 5). Therefore, the preliminary 1D throughflow performance map of the axial compressor is used to fit a parabolic function for the pressure ratio over the mass flow rate ($a_{booster} = 1.81$). The function is assumed to describe the line of maximum efficiency and hence the operating line of a corresponding axial booster design as parabolic function. By variation of the parabolic fitting factor $a_{booster}$ different booster designs are obtained in a simplified and fast way. For that, the factor is varied between $0.85 \leq a_{booster} \leq 1.90$ to cover operating strategies in both directions, higher and lower pressure ratios of the booster. Fig. 6 illustrates the achievable full-load operating lines for the variation of $a_{booster}$ at λ=3.1.

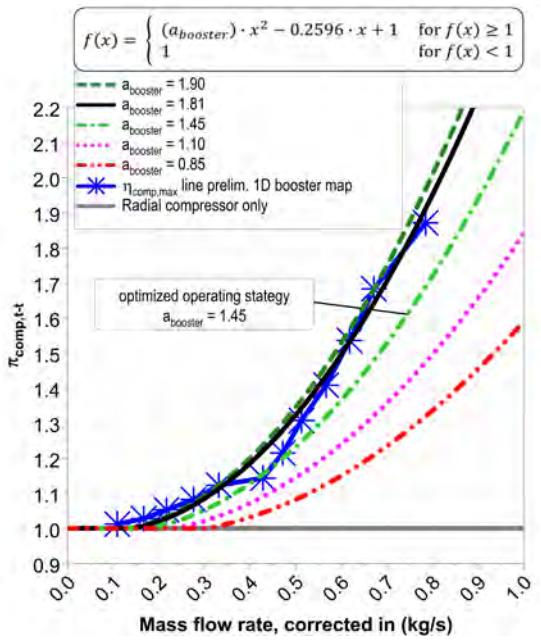

Figure 5 Operating strategies for the axial compressor.

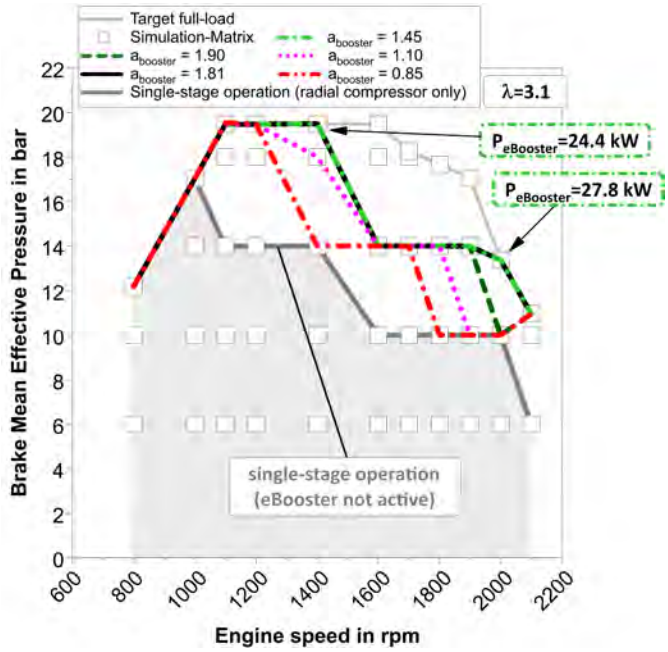

Figure 6 Full-load for different eBooster operating strategies ($\lambda = 3.1$)

The simulated points are shown by the squared markers. For this investigation no points in-between are simulated. Further, the worst case concerning the power supply for the eBooster is assumed, at which no battery functionality is taken into account (instantaneous power supply by alternator). Values of $a_{booster} \geq 1.45$ show the same full-load line until 1,900 rpm. For $a_{booster}$=1.90, compromises have to be made at 2,000 rpm due to the power limit of 35kW. For $a_{booster} \leq 1.10$, the full-load performance is degrading due to lacking pressure ratio from the booster. The best results are obtained for the labeled strategy with $a_{booster,opt} = 1.45$, which is used as the design goal in the following. At this point it remains to be said that the remaining part of the target engine map for high engine speeds and engine loads at the simulated relative air-fuel ratio of 3.1 can't be covered with this operating strategy. The presented concept offers a way to solve this issue, though. Integrating a buffer battery in between the alternator and the eBooster, electrical power could be supplied without the instantaneous parasitic losses when necessary. The required electrical energy would then have to be generated through recuperation or operating point shift at suitable engine operating points beforehand. Finally, the plot also shows the operating line at which the engine would operate at full-load when boost pressure is generated by the conventional single-stage only.

DESIGN POINT

The design point is chosen to be the upper limit of the target operating line. This is the point of highest mass flow rate and highest pressure ratio resulting in the highest power demand. This means that high efficiency in this point is essential to minimize the electrical power that needs to be provided by the engine via the alternator. It is also the operating point that is most challenging for an axial compressor because of the high pressure ratio. The design point is summarised in table 5.

Table 2 Design point for the axial compressor

Parameter	Unit	Value
Fluid	-	Air ideal gas
Mass flow rate	kg/s	0.8
Total inlet pressure	bar	1.01325
Total-total pressure ratio	-	1.72
Total inlet temperature	K	288.15
Rotational speed	rpm	77,000
Isentropic efficiency	%	87

AXIAL COMPRESSOR DESIGN

The rotor and stator preliminary design are performed in the commercial 1D blade design software AXIAL by Concepts NREC. AXIAL utilizes a reduced order throughflow solver to solve reference streamlines at hub, mid-span and tip. The tool is described in Dubitsky et al. (2003). Flow phenomena which are not modeled by this technique are accounted for by the implementation of loss models for optimal incidence, deviation, profile loss, and off-design loss. For the preliminary design presented here the modified Koch Smith loss and profile loss model (Koch and Smith Jr (1976)) with the optimal incidence and the off-design loss calculated according to AGARD (Hirsch and Denton (1981)) and the deviation according to Lieblein (Lieblein (1960)) is used. Based on the boundary conditions presented in table 5, the software calculates an initial geometry for the rotor and stator. This geometry is made up of parameters such as the blade/vane number, blade angles at hub, mid-span and tip, chord length, inlet and outlet hub and shroud diameters. For the rotor, a Multiple Circular Arc (MCA) profile is chosen because transsonic flow regime is expected for the given boundary conditions. Due to lower expected flow velocities in the stator, a Double Circular Arc (DCA) profile is chosen for the stator blade profile. After a suitable preliminary design was found, the resulting rotor and stator design was imported into the commercial 3D blade design software AxCent.

Preliminary 3D CFD results obtained with pushbutton CFD, a 3D CFD solver built into AxCent, showed that the target pressure ratio of 1.72 was not achieved by the design and that flow separation occurred in the stator. According to these results, iterative corrections were made to the preliminary design. The resulting meridional flow path is shown in figure 7 and the 3D blade design in figure 8.

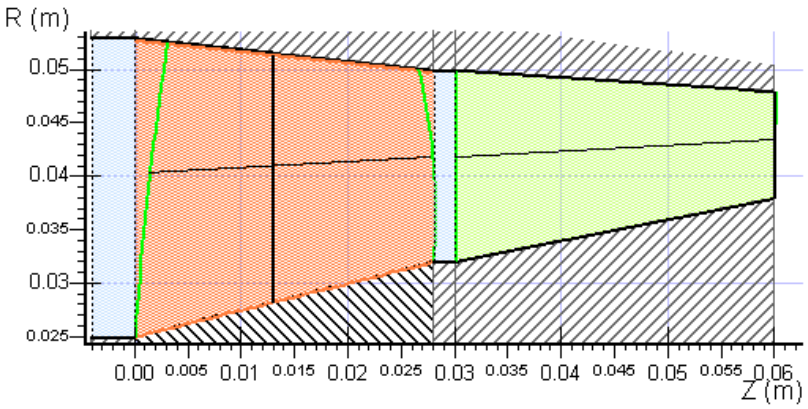

Figure 7 Final meridional flow path

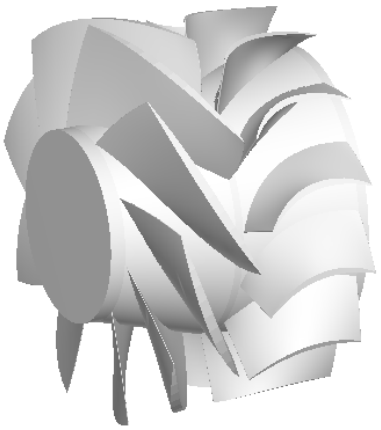

Figure 8 Final 3D blade design

The geometric parameters of the final design are summarized in table 3.

Table 3 Geometry parameters of the final compressor design

Parameter	Unit	Rotor	Stator
Blade/Vane number	-	9	13
Profile type	-	MCA	MCA
Inlet hub radius	mm	25	32
Inlet shroud radius	mm	53	50
Outlet hub radius	mm	32	38
Outlet shroud radius	mm	50	48
Tip Clearance	mm	0.2	-
Leading edge thickness	mm	0.2	0.4
Trailing edge thickness	mm	0.2	0.4
Axial chord length	mm	28	30

In order to connect the axial compressor module to the inlet pipe, the casing and the centrifugal compressor, hub bodies are needed. The commercially available centrifugal compressor has an inlet shroud diameter of 101 mm and a hub diameter of 20 mm (figure 9), resulting in a large area ratio from axial compressor stator outlet to centrifugal compressor inlet. This would require a diffuser of a length of about 500 mm which is too big due to packaging reasons. The length is limited to 200 mm and 3 struts are introduced to connect the compressor to the casing and to direct the flow. At the axial compressor inlet another hub body is introduced which is connected to the casing by 3 struts. To drive the axial compressor, a space behind the stator is introduced to hold an electric motor. The compressor's schematic setup is shown in figure 9.

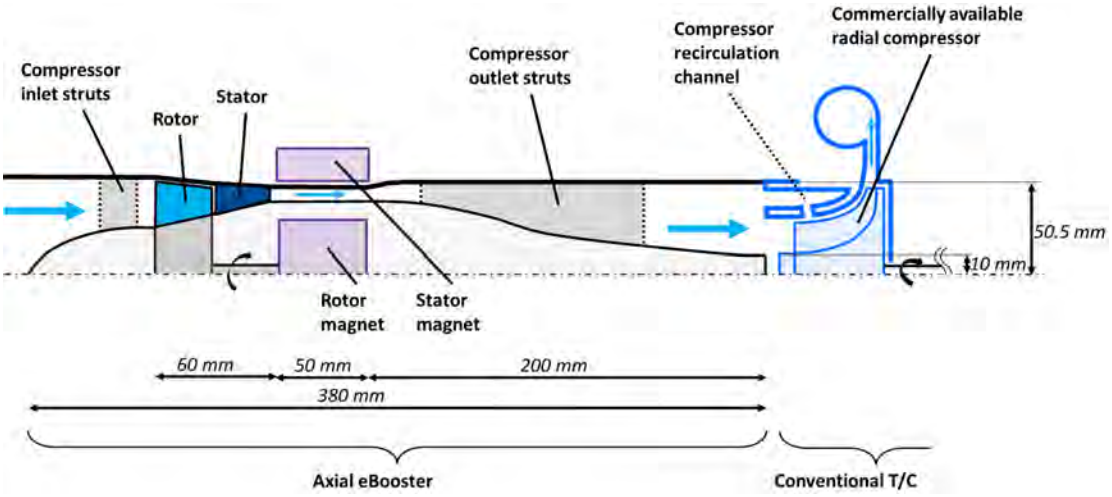

Figure 9 Schematic view of the compressor packaging

NUMERICAL SETUP

The following steady-state Reynolds-averaged Navier-Stokes (RANS) CFD simulations are performed using ANSYS CFX2022.1 (Ansys Inc (2022)). The model consists of an inlet pipe with a hub body, the compressor rotor, the stator and an outlet pipe with a hub body. All domains are modeled as periodic segments with mixing plane (constant total pressure) interfaces. The rotor and stator were meshed using ANSYS TurboGrid, and inlet and outlet pipes are meshed unstructured using ICEM CFD. In order to resolve the wall boundary layer, the first wall distance is set to ensure y^+-values below 2. The numerical setup is shown in figure 10.

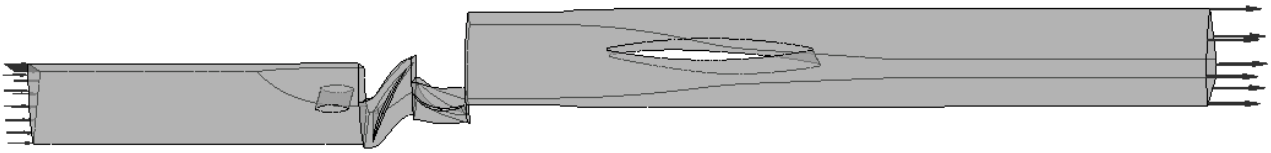

Figure 10 Numerical setup of the axial compressor

The k-ω-SST model as presented in Menter et al. (2003) is used as the turbulence model. It is shown in Simoes et al. (2009) that this model is suited best to predict the performance of an axial transsonic compressor. As separation in compressors is closely tied to laminar-turbulent transition Mayle (1991), the γ-Re$_\theta$ transition model (Menter et al. (2006)) with Kato Launder Limiter (Kato (1993)) is used. It is shown in Marciniak et al. (2013), Marciniak et al. (2014) and Langtry et al. (2006) that this model shows good agreement with experimental data. The high resolution scheme is used for the advection and turbulence schemes. The imposed boundary conditions are the total inlet pressure, the total inlet temperature, the total mass flow rate at outlet and the rotational speed. The inlet turbulent intensity is set to 5 %. The fluid is modeled as air ideal gas. For design point conditions, the outlet Reynolds number related to the hydraulic diameter is approximately 267.000.

In order to minimize the error due to the spatital discretization, a mesh independence study is performed. Three meshes are systematically refined with a refinement rate of 1.3. The grid convergence index (GCI) and the estimated relative error (EREE) are calculated regarding the total to total isentropic efficiency $\eta_{tt,is}$ according to Roache (1998). The resulting values are presented in table 4.

Table 4 Results of the mesh independence study

Grid refinement	Number of nodes	GCI in %	EREE in %
Coarse	3,192,344	2.41	1.93
Medium	7,095,938	0.13	0.11
Fine	15,109,669	0.008	0.007

For the calculations in this paper the medium mesh is chosen because the converged numerical solution has an uncertainty of $\pm$0.13 % at a confidence level of 95 % according to its GCI value.

RESULTS AND DISCUSSION

In this section, the axial compressor (rotor inlet to stator outlet) and the axial compressor module (inlet pipe inlet to outlet diffuser outlet) are evaluated numerically based on isentropic efficiency and total-to-total pressure ratio. First this is done for the design point and afterwards for the whole performance map to evaluate off-design conditions.

DESIGN POINT

The CFD results for design conditions are given in table 5, as well as the design targets. The CFD simulation of the axial compressor shows good agreement with the calculated requirements. The axial compressor itself is able to reach a slightly higher pressure ratio and efficiency than the design target. The whole module fails to meet the efficiency target because of losses occurring in the outlet diffuser. However, it is still able to deliver the pressure ratio required.

Table 5 Comparison of set and achieved compressor parameters

Parameter	Target	Axial Compressor	Module
$\eta_{tt,is}$	87 %	87 %	81.1 %
π_{tt}	1.72	1.79	1.73

The values of flow and loading coefficient and reaction for the design point are provided in Table 6. In addition, typical reference values for axial compressors in modern jet engines are provided according to Braeunling (2015). The

circumferential speed is calculated at the mean radius at rotor exit. The compressor achieves a typical value compared to the reference for flow coefficient and reaction, but shows a considerably higher loading coefficient.

Table 6 Compressor performance parameters

Parameter	Value	Reference (Braeunling (2015))
$\phi = \frac{c_m}{u}$	0.55	0.45...0.55
$\psi = \frac{\delta h_{t,comp}}{u^2}$	0.53	0.3...0.35
$\gamma = \frac{\delta h_{rot}}{\delta h_{t,comp}}$	0.72	0.5...1.0

The Mach number distribution of the axial compressor rotor and stator for design point conditions is shown for different spans in figure 11. The flow in the rotor is transsonic with Mach numbers up to 1.4 and a shock occurs at the blade tip. The contours at 90 % blade span (c) show a secondary flow vortex. Other than that, the flow is well-aligned with both rotor and the stator. The flow in the stator is subsonic with a maximum Mach number of 0.8.

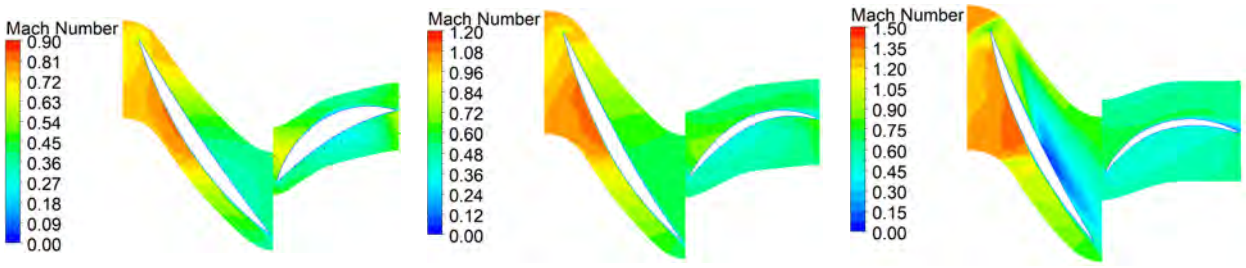

(a) 10 % span (b) 50 % span (c) 90 % span

Figure 11 Mach number contours at different spans at design point conditions

Figure 12 shows the velocity flow angle at stator outlet for design point conditions. With an angle close to 90 ° over the whole normalized span, the design goal of axial outflow is achieved.

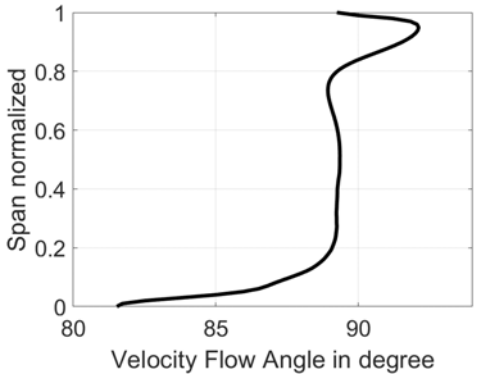

Figure 12 Velocity flow angle at stator outlet for design point conditions

Figure 13 shows the streamlines in the outlet diffuser. A large separation bubble, responsible for the decreased efficiency, occurs at the hub. The separation is caused by the large change in area in the outlet diffuser. A longer diffuser would be needed to prevent separation but this is not possible due to packaging constraints. At the design point, the outlet diffuser causes a total pressure loss of 4800 Pa.

The diffuser performance calculated according to Sovran (1967) is summarized in table 7. The overline indicates that area averaged pressures are used for the calculations. For an annular diffuser of the given area ratio, the ideal nondimensional length would need to be between 10 and 13 according to Sovran (1967). This indicates that the designed diffuser is too short, resulting in a decreased efficiency.

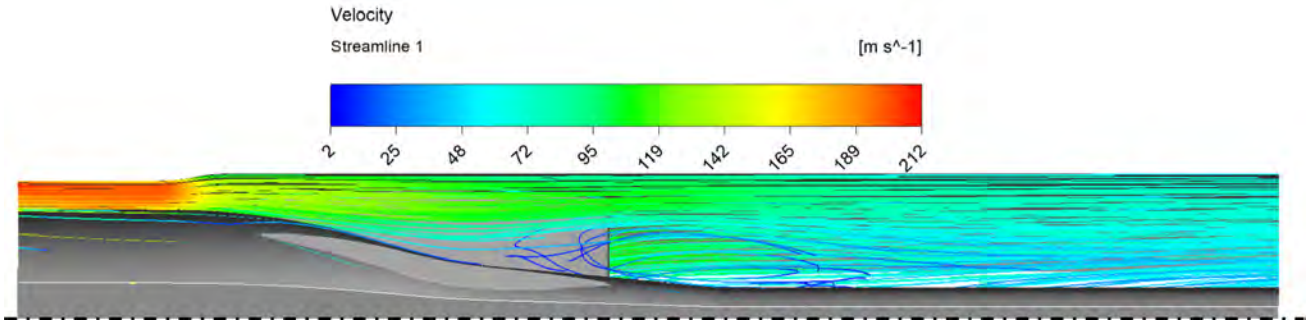

Figure 13 Streamlines in the Outlet diffuser for design point conditions

Table 7 Diffuser performance parameters

Name	Equation	Value
Area ratio	$AR=A_2/A_1$	2.85
Nondimensional diffuser length	$\hat{L} = \frac{L}{\delta R}$	4.94
Pressure recovery coefficient	$c_p = \frac{\overline{p_{out}} - \overline{p_{in}}}{\overline{p_{t,in}} - \overline{p_{in}}}$	0.637
Ideal pressure recovery coefficient	$c_{p,i} = 1 - \frac{1}{AR^2}$	0.873
Diffuser effectiveness	$\varepsilon = \frac{c_p}{c_{p,i}}$	0.726
Loss coefficient	$\Psi = \frac{\overline{p_{t,in}} - \overline{p_{t,out}}}{\overline{p_{t,in}} - \overline{p_{in}}}$	0.239

PERFORMANCE MAP

For the evaluation of compressor's performance at off-design conditions, the performance map (pressure ratio and efficiency) is calculated. The inlet total temperature is set to 288.15 K and the inlet total pressure to 1.013 bar, while the outlet mass flow rate $\dot{m}$ and the rotational speed n are altered systematically. At the surge condition, the simulation fails to converge and the last converged operating point marks the surge limit. The simulation results are illustrated in fig. 14.

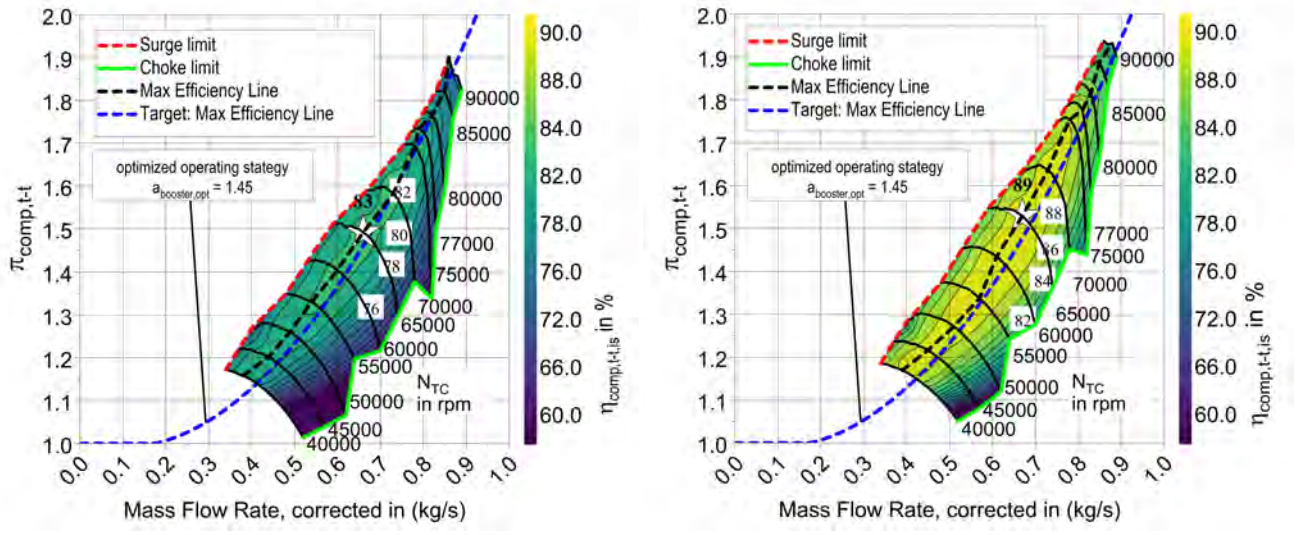

(a) Axial compressor module (entire assembly) **(b) Axial compressor (rotor-stator only)**

Figure 14 Performance maps

The performance map of the whole axial compressor module (pipe inlet to diffuser outlet) is shown in figure 14 a) and the performance map between rotor inlet and stator outlet in b). In addition, the target operating line is plotted as the black line and the line of maximum efficiency in blue. The axial compressor module shows a maximum efficiency of 83%. It is also able to cover the whole operating range from 0.4 to 0.8 kg/s corrected mass flow rate and pressure ratios of up to 1.9 with efficiencies higher than 78%. The maximum efficiency line is close to the target, highlighting the success of the design in meeting the requirements. The axial compressor (rotor-stator only) shows considerably higher efficiencies of up to 89%.

CONCLUSIONS

In the present work, a compact transsonic axial compressor is designed for charging an ultra-lean burn hydrogen combustion engine. 0/1D engine simulations are performed to determine the requirements of the charging system. CFD simulations are carried out to evaluate the performance at design conditions and to calculate the performance map.

Some of the key insights are highlighted here:

- The charging system requirements of an ultra-lean burn, inline 6-cylinder H_2-DI-SI engine at λ=3.1 show that a single-stage system is not capable to provide the necessary boost pressures. Instead a new concept featuring an axial eBooster is presented.
- When supplying the electrical energy for the eBooster directly from the crankshaft, an optimized operating strategy could be found, that can directly be used for the eBooster design process.
- Engine simulation using a is simplified eBooster show the potential of such a system to enlarge the engine operating map compared to a single-stage system. Further potential is promised by reducing instantaneous parasitic losses by the use of a buffer battery.
- The axial compressor is able to operate in the needed operating range from 0.4 to 0.8 kg/s corrected mass flow rate and to provide pressure ratios of up to 1.9.
- The axial compressor achieves high efficiencies of up to 89 % considering only the compressor (rotor inlet to stator outlet), and of up to 83% including inlet and outlet.
- Axial compressors as booster stages represent an interesting option to achieve higher boost pressures in automotive turbocharging.

Based on these findings, the next steps in the development of the charging system will be the evaluation of different outlet diffusers. A comparison between steady state and unsteady RANS is also planned. Furthermore, a suitable turbine will be designed to power the centrifugal compressor. The engine simulation tool will be used to determine the resulting performance with the presented axial booster map. Additionally, a final operating strategy for the entire charging system will be investigated in order to meet the target full-load best possible. This includes the presented possibility of providing the electrical energy not only instantaneously by the alternator, but also from a buffer battery if needed. With this planed investigation, the system can also be analysed in terms of needed battery capacity based on a specific user profile.

NOMENCLATURE

VARIABLES

$a_{booster}$ - Shape factor of parabolic function
AR - Area ratio
$BMEP$ - Break Mean Effective Pressure
C_p - pressure recovery coefficient
ε - Diffuser effectiveness
η - Efficiency
γ - Reaction
$\hat{L}$ - Nondimensional diffuser length
λ - Air-to-fuel ratio
ϕ - Flow coefficient
π - Total-to-total pressure ratio
ψ - Loading coefficient
Ψ - Diffuser loss coefficient
$\dot{m}$ - Mass flow rate
N - Rotational speed
p - Pressure
P - Power
T - Temperature

SUBSCRIPTS

comp - Compressor
cor - Corrected
engine - engine
i - ideal
in - Inlet
is - Isentropic
opt - optimized
out - Outlet
ref - Reference
rot - Rotor
t - Total

ABBREVIATIONS

CARB - California Air Resources Board
CFD - Computational Fluid Dynamics
D - Dimension
DCA - Double Circular Arc
DI - Direct injection
eBooster - Electric Booster
EERE - Estimated Extrapolated Relative Error
EM - Electric Motor
MCA - Multiple Circular Arc
RANS - Reynolds-averaged Navier-Stokes
SI - Spark Ignition
TC - Turbocharger
WaVe - Research project: Nachhaltige Wasserstoffverbrennungskonzepte (engl.: Sustainable Hydrogen Combustion)

CHEMICAL CONNECTIONS

CO_2 - Carbon dioxide
H_2 - Hydrogen
NO_X - Nitrogen oxides

ACKNOWLEDGMENTS

The investigation presented in this paper are carried out as part of the research project ”Sustainable Hydrogen Combustion” (WaVe) funded by the Lower Saxonian Ministry of Science and Culture. The research is performed at the Institute of Turbomachinery and Fluid Dynamics at the Leibniz Universitaet Hannover under the direction of Prof. Dr.-Ing. Joerg R. Seume and the Institute of Internal Combustion Engines at the Technische Universität Braunschweig under the direction of Prof. Dr.-Ing. Peter Eilts. Further, the authors gratefully thank the IAV GmbH for the granted support as well as for supplying the baseline 0/1D engine simulation model and the predictive combustion model. Finally, the results presented here were carried out on the cluster system of the Leibniz Universität Hannover, Germany, under grant. This support is gratefully acknowledged.

References

Agreement, P. (2015), Paris agreement, *in* ‘Report of the Conference of the Parties to the United Nations Framework Convention on Climate Change (21st Session, 2015: Paris). Retrived December’, Vol. 4, HeinOnline, p. 2017.

Ansys Inc (2022), ‘Ansys cfx user’s guide releases 2022.1’.

Braeunling, W. J. (2015), *Flugzeugtriebwerke: Grundlagen, Aero-Thermodynamik, ideale und reale Kreisprozesse, Thermische Turbomaschinen, Komponenten, Emissionen und Systeme*, Springer-Verlag.

California Air Resources Board (2013), ‘Heavy-duty low nox’.
URL: *https://ww2.arb.ca.gov/our-work/programs/heavy-duty-low-nox/about*

Dubitsky, O., Wiedermann, A., Nakano, T. and Perera, J. (2003), The reduced order through-flow modeling of axial turbomachinery, *in* ‘Proceedings of the International Gas Turbine Congress’, p. 8.

Fiat Powertrain (2013), ‘Fpt cursor 13 datasheet’.
URL: *https://www.fptindustrial.com/en/engines/Onroad/Trucks/XCURSOR-13-NG*

Gamma Technologies GmbH (2022), 'Gt-power user's manual, gt-suite version 2022.1'.

Heywood, J. B. (2018), *Internal combustion engine fundamentals*, McGraw-Hill Education.

Hirsch, C. and Denton, J. (1981), Through flow calculations in axial compressors, Technical report, AGARD-AR-175.

Kato, K. (1993), The modeling of turbulent flow around stationary and vibrating square cylinders, *in* 'Proc. of 9th Symp. Turbulent Shear Flows', pp. 1041–1046.

Koch, C. and Smith Jr, L. (1976), 'Loss sources and magnitudes in axial-flow compressors'.

Langtry, R. B., Menter, F., Likki, S., Suzen, Y., Huang, P. and Völker, S. (2006), 'A correlation-based transition model using local variables—part ii: test cases and industrial applications', *Journal of turbomachinery* pp. 423–434.

Lee, B., Jung, D., Assanis, D. and Filipi, Z. (2008), Dual-stage turbocharger matching and boost control options, *in* 'Internal Combustion Engine Division Spring Technical Conference', Vol. 48132, pp. 267–277.

Lieblein, S. (1960), 'Incidence and deviation-angle correlations for compressor cascades'.

Marciniak, V., Longhitano, M. and Kügeler, E. (2013), Assessment of transition modeling for the design of controlled diffusion airfoil compressor cascades, *in* 'Turbo Expo: Power for Land, Sea, and Air', Vol. 55225, American Society of Mechanical Engineers, p. V06AT35A016.

Marciniak, V., Weber, A. and Kügeler, E. (2014), Modelling transition for the design of modern axial turbomachines, *in* 'Proceedings of the 6th European Conference on Computational Fluid Dynamics, Barcelona, Spain', pp. 20–25.

Mayle, R. E. (1991), 'The 1991 igti scholar lecture: the role of laminar-turbulent transition in gas turbine engines'.

Menter, F. R., Kuntz, M. and Langtry, R. (2003), 'Ten years of industrial experience with the sst turbulence model', *Turbulence, heat and mass transfer* **4**(1), 625–632.

Menter, F. R., Langtry, R. B., Likki, S., Suzen, Y., Huang, P. and Völker, S. (2006), 'A correlation-based transition model using local variables—part i: model formulation', *Journal of turbomachinery* **128**(3), 413–422.

Onorati, A., Payri, R., Vaglieco, B., Agarwal, A., Bae, C., Bruneaux, G., Canakci, M., Gavaises, M., Günthner, M., Hasse, C. et al. (2022), 'The role of hydrogen for future internal combustion engines'.

Oung, R., Foucher, F., Neveu, J., Vucher, A. and Rieser, E. (2022), 'H2 efficient and near zero emissions operation on a pfi hd single cylinder diesel ice'.

Plötz, P., Wachsmuth, J., Gnann, T., Neuner, F., Speth, D. and Link, S. (2021), 'Net-zero-carbon transport in europe until 2050—targets, technologies and policies for a long-term eu strategy', *Karlsruhe: Fraunhofer Institute for Systems and Innovation Research ISI. Available online: https://www. isi. fraunhofer. de/en. html (accessed on 25 July 2021)* .

Rezaei, R., Hayduk, C., Fandakov, A., Rieß, M., Sens, M. and Delebinski, T. O. (2021), Numerical and experimental investigations of hydrogen combustion for heavy-duty applications, Technical report, SAE Technical Paper.

Rieß, M., Fandakov, A., Wolany, A. and Wöbke, M. (2021), 'Phenomenological modeling of h2 combustion', *MTZ worldwide* **82**(10), 16–21.

Roache, P. J. (1998), *Verification and validation in computational science and engineering*, Vol. 895, Hermosa Albuquerque, NM.

Simoes, M. R., Montojos, B. G., Moura, N. R. and Su, J. (2009), Validation of turbulence models for simulation of axial flow compressor, *in* '20th international congress of mechanical engineering'.

Sovran, G. (1967), 'Experimentally determined optimum geometries for rectlinear diffusers with rectangular, conical or annular cross section', *Fluid mechanics of internal flow* pp. 270–319.